Article

Human–Machine Redundant Braking System for Aftermarket Low-Speed Electric Vehicle: Design and Validation

Shulei Sun [1,2], Wei Qu [1], Xiaorong Huang [1,2,*], Guoying Tian [1], Pengyi Deng [1], Kunfan Liu [1], Yan Tang [3], Liang Chen [1] and Chongfeng Wei [4,*]

1 Vehicle Measurement, Control and Safety Key Laboratory of Sichuan Province, Xihua University, Chengdu 610039, China; shuleisun@foxmail.com (S.S.); 0120150032@mail.xhu.edu.cn (G.T.); 0120130027@mail.xhu.edu.cn (P.D.)
2 Provincial Engineering Research Center for New Energy Vehicle Intelligent Control and Simulation Test Technology of Sichuan, Xihua University, Chengdu 610039, China
3 China Industry Innovation Alliance for the Intelligent and Connected Vehicles, Beijing 102607, China
4 School of Mechanical and Aerospace Engineering, Queen's University Belfast, Belfast BT9 5AG, UK
* Correspondence: 1220190017@mail.xhu.edu.cn (X.H.); c.wei@qub.ac.uk (C.W.)

Abstract: This paper presents the design and experimental validation of a novel human–machine redundant braking system (HMRBS) for aftermarket low-speed electric vehicles (LSEVs) to realise the backup redundancy ability and improve active safety. First, the HMRBS is designed by connecting the electro-hydraulic braking (EHB) unit oil pipelines in parallel with the manual braking (MB) unit through two three-way shuttle valves. Then, the mathematical model of the EHB subsystem is built, and a master cylinder pressure controller with adaptive fuzzy proportion integration differentiation (PID) and a servo motor speed controller with double-closed-loop proportion integration (PI) are proposed to improve the system response performance. Following this, the co-simulation model of the proposed closed-loop system is established based on AMESim and MATLAB/Simulink to validate the feasibility of the proposed control strategy. Finally, the effectiveness of the HMRBS is also validated by test rig and vehicle experiments. The results imply that the modified LSEV with the HMRBS meets the requirements of vehicle active braking ability and manual braking redundancy. Furthermore, the proposed controller can significantly enhance pressure control accuracy compared to the classical PID controller. The deceleration fluctuation and braking distance in the active braking mode are smaller than those in the manual braking mode, indicating that the proposed system makes the braking effect more stable and safer.

Keywords: low-speed electric vehicle; redundant braking system; EHB system; structural scheme design; experimental validation; pressure control

1. Introduction

Electrification and intelligence are currently emerging as global trends in the vehicle industry. Brake-by-wire technology has been greatly developed and applied to vehicle active braking systems [1–3]. With the help of the active braking system, intelligent vehicles equipped with advanced driver assistance systems (ADAS), e.g., adaptive cruise control (ACC) and autonomous emergency braking (AEB), can significantly improve driving safety [4–6].

Currently, more and more passenger and commercial vehicles are equipped with brake-by-wire systems. However, most LSEVs, such as electric sightseeing vehicles, street sweepers, or light electric logistics vehicles that run on fixed routes or in closed scenes, have not been equipped with brake-by-wire systems due to the low quantity, high development costs, and various customised requirements [7]. In addition, the different mechanical structures and vehicle dynamic performance requirements increase the development difficulty. The brake-by-wire systems should be designed, matched, calibrated, and debugged

according to different types of vehicles. Therefore, it is necessary to develop an automatic braking system with a simple structure, high reliability, low cost, easy modification, and low debugging difficulty to improve the active braking capability of LSEVs.

Electro-hydraulic braking (EHB) systems are currently the mainstream active braking mode used in intelligent vehicles [8,9]. Some EHB products have been successfully developed, such as the MKC1 and iBooster [10,11]. Meanwhile, many scholars are also constantly improving and optimising the structure of the EHB system, e.g., a master cylinder based on the speed servo system with an anti-lock function [12], and a dual redundant brake-by-wire for highly automated driving safety [13]. A redundancy braking system with EHB has the ability to activate the vehicle's emergency and consistency brake, even if the brakes are not activated due to electrical or mechanical failures or external shocks [14]. However, the application object of all the above EHB systems is mass-produced new passenger or commercial vehicles, which makes them unsuitable for use in the aftermarket LSEVs to achieve active braking function.

EHB control strategies play a critical role in braking performance and safety. Recent literature shows increasing interest in EHB control strategies. A double-closed-loop PI feedback control system was proposed to obtain a better position–pressure relationship, where the inner loop and outer loop control the position and pressure, respectively [15]. However, the characteristics of the brake oil, the friction, and the large transmission ratio of the transmission mechanism will cause strong nonlinearity, thereby affecting the robustness of the controller [13,16]. A fuzzy PI controller for the hydraulic pressure control of the master cylinder was designed to improve the robustness of the PI control method [17–19]. A sliding mode control method of the electro-hydraulic brake master cylinder pressure was proposed, aiming at the nonlinear problems such as oscillation and low-speed creeping of the master cylinder in the control process [20]. However, the position of the master cylinder piston is not considered in the fuzzy PI or sliding mode controller, resulting in low control accuracy. Therefore, it is necessary to design a controller with fast response, high reliability, and low cost to ensure the master cylinder pressure accuracy and stability of the EHB system.

Aiming at these problems, a novel human–machine redundant braking system (HMRBS) is proposed in this paper, and its innovation points are as follows:

1. On the premise of retaining the original braking system of LSEV, a low-cost HMRBS is designed by connecting the oil pipelines of the EHB unit in parallel with the manual braking (MB) unit through two three-way shuttle valves. As a result, the HMRBS has two braking modes, active and manual braking modes, thus ensuring the redundancy of braking backup.

2. The HMRBS mathematical model is established, and the master cylinder pressure controller with adaptive fuzzy PID and the servo motor speed controller with double-closed-loop PI are designed. Moreover, a test rig is developed, and an LSEV is modified with the HMRBS. Finally, the effectiveness of the proposed braking system is validated by experiments.

The rest of this paper is organised as follows. Section 2 illustrates the structure design scheme, operating principles, and mathematical model. Section 3 introduces the controller design of the HMRBS. In Section 4, the co-simulation results are given to verify the effectiveness of the proposed scheme. The experiments are carried out on a test rig and modified test LSEV, respectively, in Section 5. Finally, several conclusions are given in Section 6.

2. Design Scheme and Mathematical Model

2.1. Design Scheme

Figure 1 shows the schematic of the human–machine redundant braking system (HMRBS) proposed in this paper. The system mainly comprises the MB unit, the EHB unit, and the wheel cylinder braking (WCB) unit. The EHB unit is connected in parallel to the original vehicle braking system (i.e., MB unit) through two three-way shuttle valves.

The MB unit is consistent with the original vehicle system without any changes. It has the advantage of having a simple structure, high reliability, low cost, easy modification, and low debugging, especially for vehicles in the aftermarket. Therefore, the HMRBS has two braking modes: active braking mode and manual braking mode. The HMRBS works as follows:

1. Active braking mode: First, the EHB subsystem receives the braking pressure request signal via the controller area network (CAN) from upper intelligent driving systems. Then, the torque output by the brushless DC motor (BLDCM) is increased via the worm gear reducer (WGR). Meanwhile, the rotary motion of the worm gear is converted into the translational motion of the pushrod of the master cylinder 1 (MC1) through the ball screw mechanism (BSM). The high-pressure oil from MC1 enters the two three-way shuttle valves, i.e., SV1 and SV2, and the valve cores of SV1 and SV2 will move to the right. The independent oil circuit system comprises EHB and WCB units in this mode. Finally, the oil enters the brake caliper and increases the braking pressure.

2. Manual braking mode: In this mode, the oil pressure of the master cylinder 2 (MC2) increases under the action of the foot pedal force, lever mechanism, and vacuum booster (some LSEVs do not have any vacuum booster). Then, the valve cores move to the left so that the MB and WCB units form an independent oil circuit system. The manual braking mode normally works even if the active braking fails. Therefore, the HMRBS can improve vehicle braking safety.
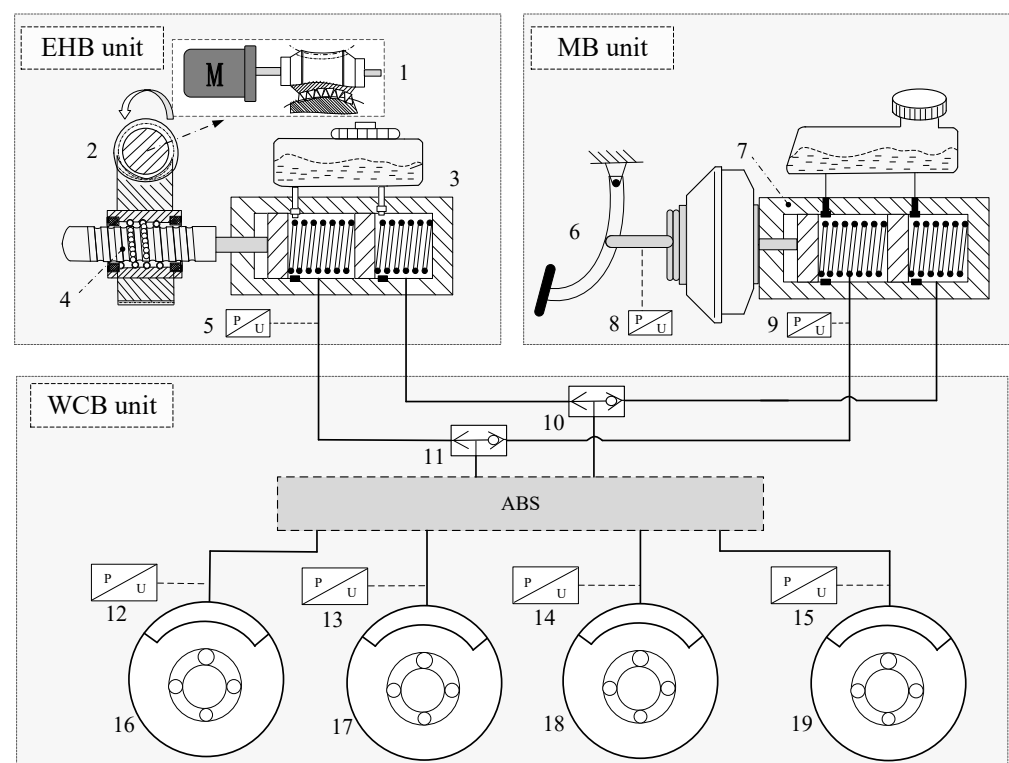
1—Brushless DC motor (BLDCM); 2—Worm gear reducer (WGR); 3—EHB master cylinder (MC1); 4—Ball screw mechanism (BSM); 5—Pressure sensor 1 (PS1); 6—Brake pedal (BP); 7—Manual braking master cylinder (MC2); 8—Pedal displacement sensor (PDS); 9—Pressure sensor 2 (PS2); 10—Three-way shuttle valve 1 (SV1); 11—Three-way shuttle valve 2 (SV2); 12—Pressure sensor 3 (PS3); 13—Pressure sensor 4 (PS4); 14—Pressure sensor 5 (PS5); 15—Pressure sensor 6 (PS6); 16—Caliper assembly-front left (FL); 17—Caliper assembly-rear right (RR); 18—Caliper assembly-front right (FR); 19—Caliper assembly-rear left (RL)

Figure 1. The design schematic of the HMRBS.

2.2. Mathematical Model

A mathematical model of the system is required for the subsequent co-simulation and controller design to validate the feasibility of the design scheme. Therefore, the mathematical models of BLDCM, transmission mechanism, brake master cylinder, wheel cylinder, and brake line are developed in this paper.

The electromagnetic torque of BLDCM can be expressed as [21]

$$T_e = \frac{P_e}{\omega} = \frac{1}{\omega}(e_a i_a + e_b i_b + e_c i_c) \tag{1}$$

where P_e stands for electromagnetic power of the motor, T_e is electromagnetic torque, and ω is motor angular speed. i_a, i_b, and i_c are the phase currents of three-phase stator windings, respectively. e_a, e_b, and e_c are the back-EMF of three-phase stator windings.

The motor kinematic equation can be obtained by

$$T_e - T_L - B_v \omega = J\frac{d\omega}{dt} \tag{2}$$

where T_e is electromagnetic torque, T_L is the additional load torque, and B_v is the damping coefficient.

The dynamics model of the master cylinder can be written as

$$M_{m1}\ddot{x}_1 + k_{m1}(x_1 - x_2) + c_{m1}(\dot{x}_1 - \dot{x}_2) = F_m - P_{m1}A \tag{3}$$

$$M_{m2}\ddot{x}_2 + k_{m2}x_2 + c_{m2}\dot{x}_2 + p_{m2}A = k_{m1}(x_1 - x_2) + c_{m1}(\dot{x}_1 - \dot{x}_2) + p_{m1}A \tag{4}$$

where M_{m1} and M_{m2} stand for the mass of the front piston and the rear piston, respectively. x_1 and x_2 stand for the displacement of the front piston and the rear piston, respectively. c_{m1} and c_{m2} are the respective spring damping coefficients. k_{m1} and k_{m2} are the respective spring stiffness. p_{m1} and p_{m2} stand for the pressure of the front and rear chambers, respectively. A is the cross-sectional area of the piston.

The continuity equation of hydraulic transmission of the master cylinder can be written as [22]

$$\dot{p}_{m1} = \begin{cases} 0 & x_1 \leq d_1 \\ \frac{\beta(A\dot{x}_1 - A\dot{x}_2 - Q_{m1})}{V_{m1} - A(x_1 - d_1) + A(x_2 - d_2)} & x_1 > d_1 \end{cases} \tag{5}$$

$$\dot{p}_{m2} = \begin{cases} 0 & x_2 \leq d_2 \\ \frac{\beta(A\dot{x}_2 - Q_{m2})}{V_{m2} - A(x_2 - d_2)} & x_2 > d_2 \end{cases} \tag{6}$$

where β is the equivalent volume elastic modulus of the brake oil. V_{m1} and V_{m2} are the volumes of chambers after the front and rear pistons are compensated, respectively. d_1 and d_2 are the compensation displacement of the front and rear chambers, respectively. Q_{m1} and Q_{m2} are the flow of the front and rear chamber brake lines, respectively.

The model of the wheel cylinder can be expressed as [23]

$$M_w \ddot{x}_w = A_w p_s - F_s - c_w \dot{x}_w \tag{7}$$

$$F_s = k_w(x_{q1} + x_{q0}) \tag{8}$$

$$x_{q1} A_w = \int_0^t Q_v dt \tag{9}$$

The continuity equation of the hydraulic pressure change of the wheel cylinder can be expressed as

$$\dot{p}_w = \beta \frac{Q_v - \dot{V}_w(x_w)}{V_w(x_w)} \tag{10}$$

$$V_w(x_w) = (L_w + x_w)A_w \tag{11}$$

where M_w is the mass of the caliper and x_w is the equivalent displacement of the rigid body. A_w is the cross-sectional area of the wheel cylinder piston, p_s is the oil pressure on the piston, k_w is the equivalent stiffness of the spring in the initial state of the piston, c_w is the damping coefficient of the wheel cylinder, x_{q0} is the equivalent preload of spring, x_{q1} is the equivalent displacement of the rigid body, Q_v is the brake oil flow, and L_w is the initial liquid width of the wheel cylinder.

The continuity equation of the brake line can be written as

$$Q_P = \frac{V_p}{\beta} \frac{dP_p}{dt} \tag{12}$$

where Q_p is the flow in the brake line, P_p is the actual pressure in the brake line, V_p is the volume of the brake hose, and β is the equivalent volumetric elastic modulus of brake oil.

The parameters involved in the EHB unit are shown in Table 1.

Table 1. Parameter in the EHB unit.

Parameters	Value
WGR transmission ratio (i)	15
Front/rear piston mass (M_{m1})	0.3 kg
Stiffness of front chamber spring (k_{m1})	7 N/mm
Stiffness of rear chamber spring (k_{m2})	4 N/mm
Inner diameter of master cylinder (d_m)	23.8 mm
Damping coefficients (c_m)	0.01 N/(mm/s)
Equivalent volumetric elastic modulus of brake oil (β)	1700 MPa
Front brake wheel cylinder diameter (D_{wf})	57 mm
Rear brake wheel cylinder diameter (D_{wr})	23 mm
Front brake piston mass (M_{wf})	0.75 kg
Rear brake piston mass (M_{wr})	0.4 kg
Equivalent contact stiffness of wheel cylinder (k_w)	2.3×10^7 N/m
Wheel cylinder damping coefficient (c_w)	10,000 N/(m/s)
Brake oil density (ρ)	850 kg/m^3
Inner diameter of brake hard tube (D_{ph})	3.3 mm
Inner diameter of brake hose (D_{ps})	3.3 mm

3. Controller Design

The HMRBS can realise the independent parallel control of the EHB and MB units. When the vehicle encounters an emergent event, the driver can brake the vehicle by MB unit. If the driver does not notice the emergency, the vehicle can be braked automatically by the EHB unit based on the control strategy. Therefore, the controller of the EHB unit of the HMRBS should be designed to meet braking safety. In the controller design, the master cylinder pressure-tracking performance and control accuracy should be guaranteed [24].

A closed-loop control strategy of the EHB unit is proposed in this paper, including the master cylinder pressure controller with adaptive fuzzy PID and the servo motor speed controller with double-closed-loop PI, shown in Figure 2. k_p, k_i, and k_d are PID control parameters. Δk_p, Δk_i, and Δk_d are the variations of the PID control parameters. P_{tar} is target pressure, P_{act} actual pressure, u_{tar} target voltage, u_{act} actual voltage, i_{tar} target current, and i_{act} actual current.
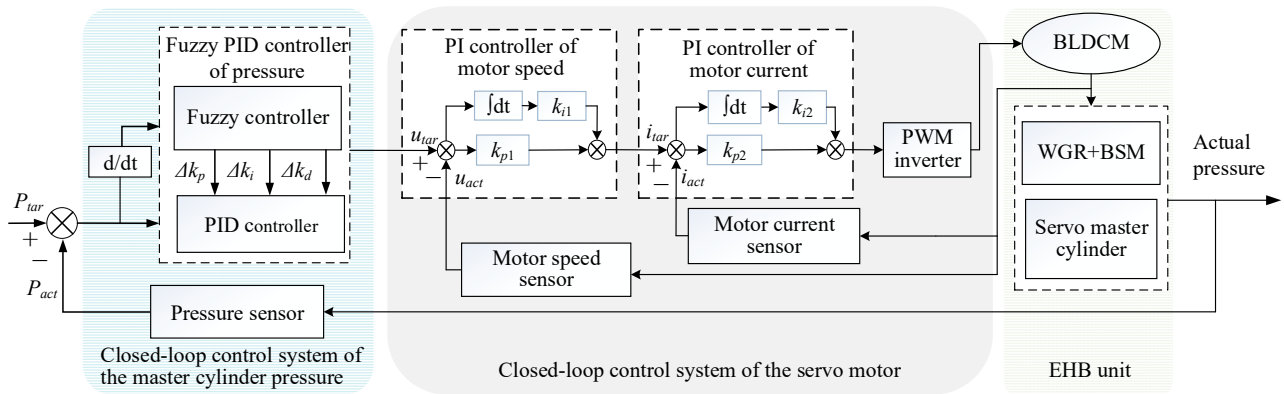
Figure 2. Closed-loop control strategy of EHB unit pressure.

3.1. Master Cylinder Pressure Controller Design

In the master cylinder (MC1) pressure controller with adaptive fuzzy PID, the error between the expected pressure and the actual pressure and its change rate are the input signals, and the output is the expected speed of the servo motor.

The initial fuzzy PID parameters are set to $k_p = 11$, $k_i = 1.5$, and $k_d = 1.1$. The deviation between the actual master cylinder pressure value obtained by the pressure sensor and the target pressure value sent by the upper controller can be expressed as $e = P_{act} - P_{tar}$, and its rate of change can be expressed as $e_c = d_e/d_t$.

The variables are scaled into the integer discourse domain range of $[-6, 6]$, and both concrete subsets of numbers are $\{-6, -4, -2, 0, 2, 4, 6\}$. The fuzzy set corresponding to the basic domain is set to {NB NM NS ZO PS PM PB}. The discourse domain of input variables is divided into seven membership functions: NB (Negative Big), NM (Negative Middle), NS (Negative Small), ZO (Zero), PS (Positive Small), PM (Positive Middle), and PB (Positive Big). Fuzzification of the theoretical domains of e and e_c yields a mainly triangular affiliation function, as shown in Figure 3.
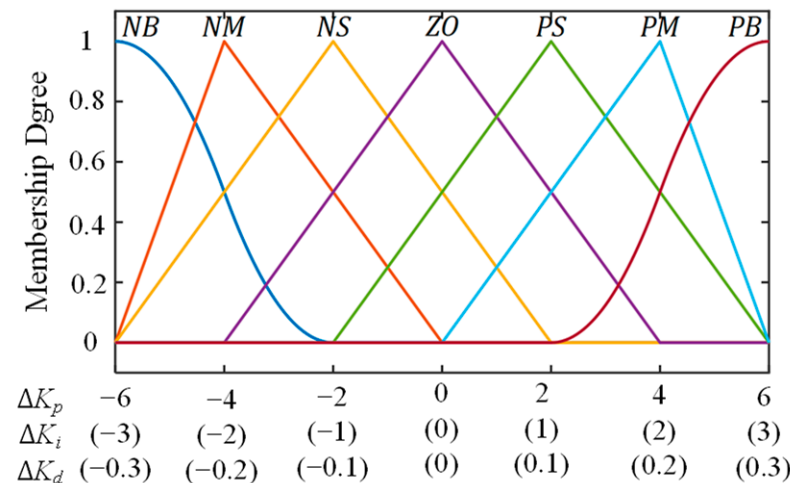

Figure 3. Membership function of inputs.

The output of the adaptive fuzzy PID controller consists of three correction terms, Δk_p, Δk_i, and Δk_d, which modify the PID control parameters k_p, k_i, and k_d, respectively. The domains and fuzzy subsets for these output terms are defined as follows: the domain of Δk_p is $\{-6, -4, -2, 0, 2, 4, 6\}$, the domain of Δk_i is $\{-3, -2, -1, 0, 1, 2, 3\}$, and the domain of Δk_d is $\{-0.6, -0.4, -0.2, 0, 0.2, 0.4, 0.6\}$. Correspondingly, the fuzzy sets are {NB, NM, NS, ZO, PS, PM, PB}, with a quantification factor of 1 for each term. The membership function type of the input and output variable is mainly triangular, and the membership function is obtained after fuzzification, as shown in Figure 4.
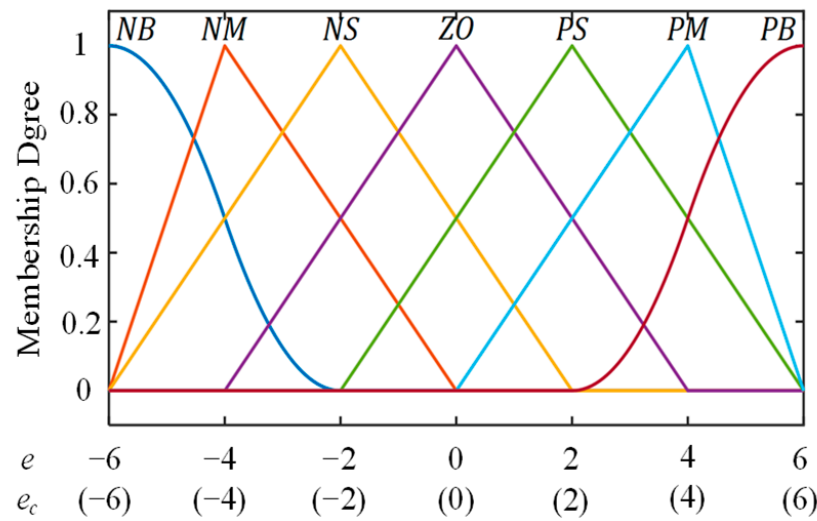
Figure 4. Membership function of outputs.

Adaptive fuzzy PID control applies the modern control theory to set the parameters of the online controlled object, making the control system adapt to the requirements constantly to achieve better control effects. The formulation of fuzzy control rules requires the integration of the PID parameter-tuning experience. The three parameters, Δk_p, Δk_i, and Δk_d, can be set reasonably and dynamically [25]. Referencing the values of input variables e and e_c, adjustments are made to the magnitudes of Δk_p, Δk_i, and Δk_d. During the initial adjustment phase, the error and the error rate between the actual and desired pressure values are relatively high, so a larger Δk_p is chosen to obtain a higher system response rate. A smaller Δk_d is selected to prevent differential saturation, and the integral effect is somewhat weakened. In the middle stage of adjustment, when the values of pressure difference e and its rate of change e_c are moderate, the initial value of Δk_p can be appropriately reduced to control the system with minimal overshoot while ensuring a reasonable response rate. To maintain stability, Δk_i, and Δk_d are kept relatively moderate and unchanged. In the later stage, to improve the pressure-tracking stability, Δk_p is increased appropriately, and the integral action is intensified to reduce steady-state error and enhance control accuracy. Considering the sensitivity of the system pressure controller to changes in the k_d parameter, Δk_d should be reduced to compensate for the prolonged adjustment process caused by the larger Δk_p value during the initial adjustment phase. Based on the aforementioned parameter adjustment experience, the fuzzy rules are summarised in Table 2.

Table 2. Fuzzy control rule table.

	Values of Δk_p, Δk_i, and Δk_d for Different Pressure Deviation e and Change Rate e_c						
e \ e_c	**NB**	**NM**	**NS**	**ZO**	**PS**	**PM**	**PB**
NB	PB/NB/PS	PB/NB/NS	PM/NM/NB	PM/NM/NB	PS/NS/NB	ZO/ZO/NM	ZO/ZO/PS
NM	PB/NB/PS	PB/NB/NS	PM/NM/NB	PS/NS/NM	PS/NS/NM	ZO/ZO/NS	NS/ZO/ZO
NS	PM/NB/ZO	PM/NM/NS	PM/NS/NM	PS/NS/NM	ZO/ZO/NS	NS/PS/NS	NS/PS/ZO
ZO	PM/NM/ZO	PM/NM/NS	PS/NS/NS	ZO/ZO/NS	NS/PS/NS	NM/PM/NS	NM/PM/ZO
PS	PS/NM/ZO	PS/ZO/NS	ZO/ZO/ZO	NS/PS/ZO	NS/PS/ZO	NM/PM/ZO	NM/PB/ZO
PM	PS/ZO/PB	ZO/ZO/NS	NS/PS/PS	NM/PS/PS	NM/PM/PS	NM/PB/PS	NB/PB/PB
PB	ZO/ZO/PB	ZO/ZO/PM	NM/PS/PM	NM/PM/PM	NM/PM/PS	NB/PB/PS	NB/PB/PB

Δk_p, Δk_i, and Δk_d obtained by fuzzy reasoning are a fuzzy set which cannot calibrate the parameters. Therefore, the fuzzy set should be converted into an actual value that can be recognised by the control system [26]. The centroid method is chosen for defuzzification, and can be expressed as

$$u = \frac{\sum\limits_{i=1}^{n} M(u_i)u_i}{\sum\limits_{i=1}^{n} M(u_i)} \tag{13}$$

where u_i is an element of the domain $\{u_1, u_2 \ldots \ldots u_i\}$, and $M(u_i)$ is the value of the membership function when $u = u_i$.

3.2. Servo Motor Speed Controller Design

The rapid response and accurate control of the target signal should be accomplished in the servo motor speed controller with double-closed-loop PI. The motor speed loop is set to the outer loop, and the current loop of the motor is set to the interior loop, respectively.

In the outer loop, the input variable is the difference between the expected and actual speed, and the prospective current of the motor is chosen as the output. The difference between the prospective current and the actual motor current obtained by the current sensor is taken as the input variable of the current interior loop PI controller. Subsequently, the output signal is used as the input of the duty ratio of the PWM inverter. Control of PWM can be achieved by adjusting the duty ratio. Finally, the servo motor is driven to forward or reverse motion, and then the master cylinder piston is pushed or pulled by the transmission mechanism to achieve pressure control.

The principle behind pulse width modulation (PWM) is to compare the waveform (modulating wave) synthesised by the required sawtooth/triangular wave (carrier wave) with a reference voltage and determine the polarity of the PWM output. When the sawtooth wave is fed into the inverting input of the comparator and exceeds the reference voltage, the output polarity is the opposite of the sawtooth wave. When the sawtooth wave is fed into the non-inverting input of the comparator and exceeds the reference voltage, the output polarity is the same as the sawtooth wave.

## 4. Simulation and Discussion

4.1. Co-Simulation Model

A co-simulation model of the HMRBS is built with MATLAB/Simulink and AMESim to validate the feasibility of the control algorithm of master cylinder pressure tracking. The EHB unit consists of the controller sub-model and the hydraulic mechanism sub-model. The controller sub-model is developed in MATLAB/Simulink software based on the closed-loop control strategy. The hydraulic mechanism sub-model includes the transmission mechanism, brake master cylinder, brake wheel cylinder, and brake pipeline, accomplished in AMEsim software. The exchange of data of the master cylinder pressure and target motor torque is realised in the co-simulation, shown in Figure 5.
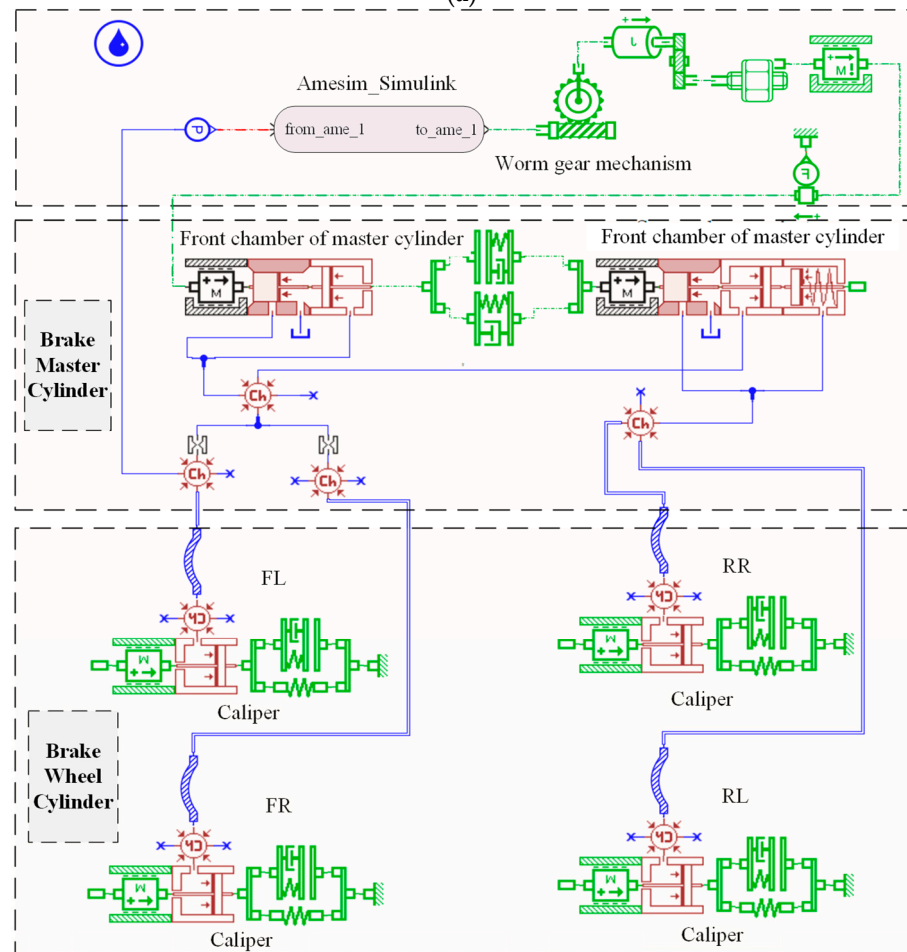
4.2. Simulation Results

The classical PID and fuzzy PID strategies are compared and analysed in co-simulation. Two signal-inputting simulation conditions are used as follows: (1) a step signal with 6 MPa at 0.5 s; (2) a sine signal with an offset of 3 MPa, an amplitude of 3 MPa, and a frequency of 1 Hz. The results are displayed in Figures 6 and 7.

Figure 6 shows the results of the case with the step signal. The simulation case can evaluate the transient response of rapid pressurisation, rapid decompression, and pressure-holding capacity of the master hydraulic pressure under emergency active braking conditions. The rise time of PID and fuzzy PID is almost the same. The overshoot of PID is 0.26 MPa, and the steady-state error is 0.05 MPa. The overshoot of the fuzzy PID proposed is 0.18 MPa, and the steady-state error is 0.04 MPa, which are reduced by 42% and 20%, respectively.
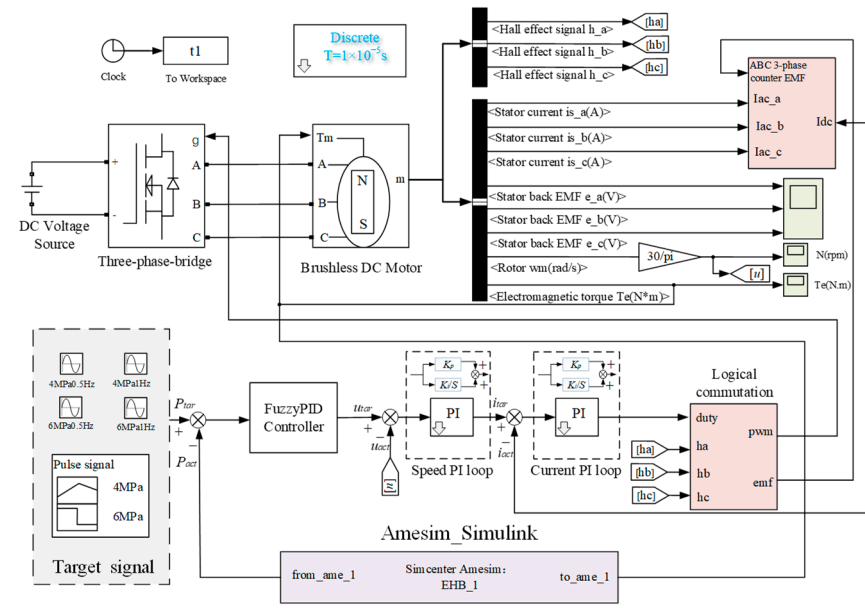
Figure 5. The co-simulation model of the EHB unit of HMRBS: (**a**) the controller sub-model in Matlab/Simulink; and (**b**) hydraulic mechanism sub-model in AMESim.
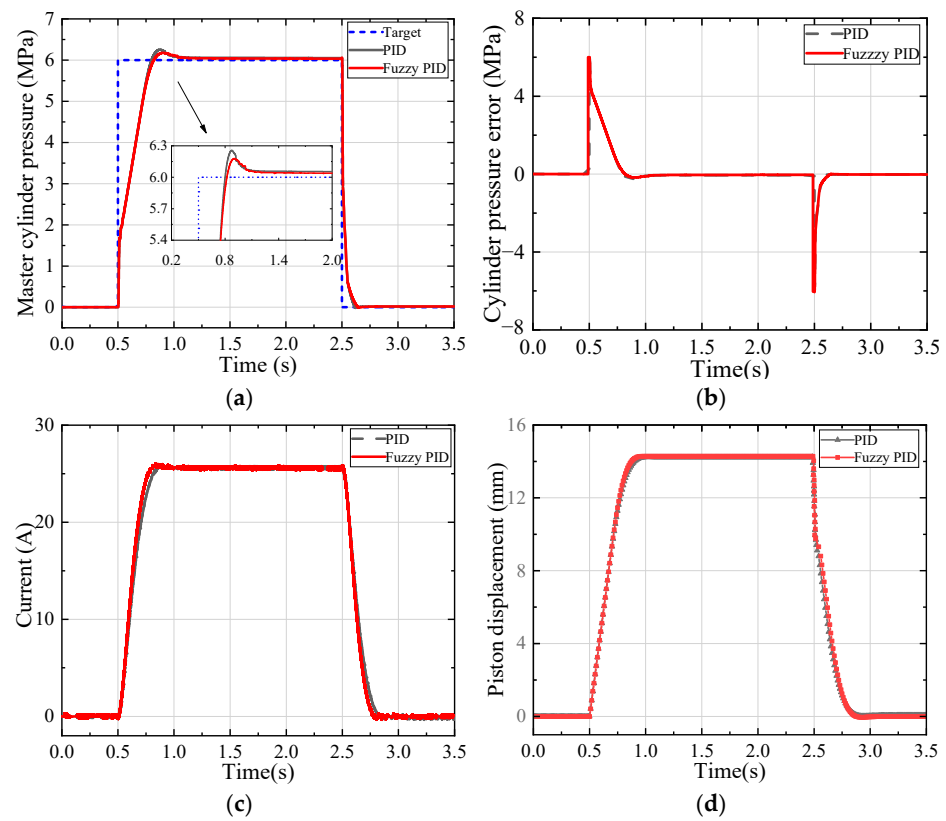
Figure 6. The step target pressure-tracking simulation results: (**a**) pressure-tracking curve; (**b**) pressure error curve; (**c**) electric current curve; and (**d**) piston displacement curve.
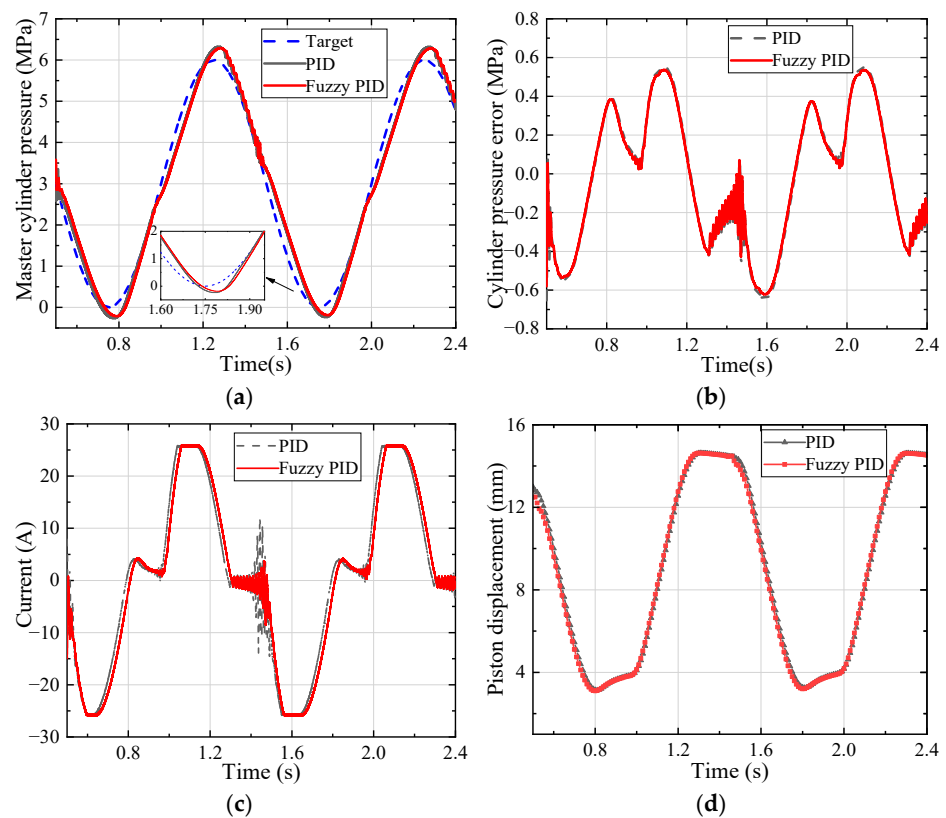

Figure 7. The sinusoidal signal target pressure-tracking simulation results: (**a**) pressure-tracking curve; (**b**) pressure error curve; (**c**) electric current curve; and (**d**) piston displacement curve.

Figure 7 shows the results of the case with the sine signal. The simulation case can validate the dynamic response of the HMRSB under the periodically changing target pressure. The maximum tracking error of PID is 0.65 MPa, while the error of fuzzy PID is 0.62 MPa, which is reduced by 4.6%.

Therefore, the fuzzy PID proposed in this paper is superior to PID in overshoot, steady-state errors, and tracking errors. The results prove the effectiveness and accuracy of the fuzzy PID control strategy.

5. Test and Discussion

5.1. Test Rig Results

Compared with the simulation analysis, the actual system has uncertainties such as parameter variations, modeling errors, and external disturbances. Therefore, the robustness of the proposed method can be proved by rig and vehicle experiments. A brake system hardware-in-the-loop (HIL) test rig is built to evaluate the dynamic pressure characteristics of the HMRBS, as shown in Figure 8. The detailed specifications are listed in Table 3. A pressure controller is constructed in MATLAB/Simulink to receive the desired pressure value as input and generate the desired speed for the servo motor. The desired speed of the servo motor is then sent to the motor controller via the CAN Bus analyser. After passing through the motor speed controller and current controller, the motor control torque is outputted to achieve speed control of the motor, thereby driving the master cylinder piston to operate and complete the electro-hydraulic braking. The control code is developed based on the feedback signals from the current sensor and speed sensor in the motor to meet different control performance requirements. The time–pressure target signals of step tests and sine sweep tests are carried out in this paper. In the step tests, the system is sent step signals with amplitude of 4 MPa and 6 MPa; in the sine sweep tests, the sine signals with an offset of 3 MPa and 2 MPa, an amplitude of 3 MPa and 2 MPa, and a frequency of 0.5 Hz and 1Hz are input. The transient response and holding capacity of the master cylinder pressure were acquired.
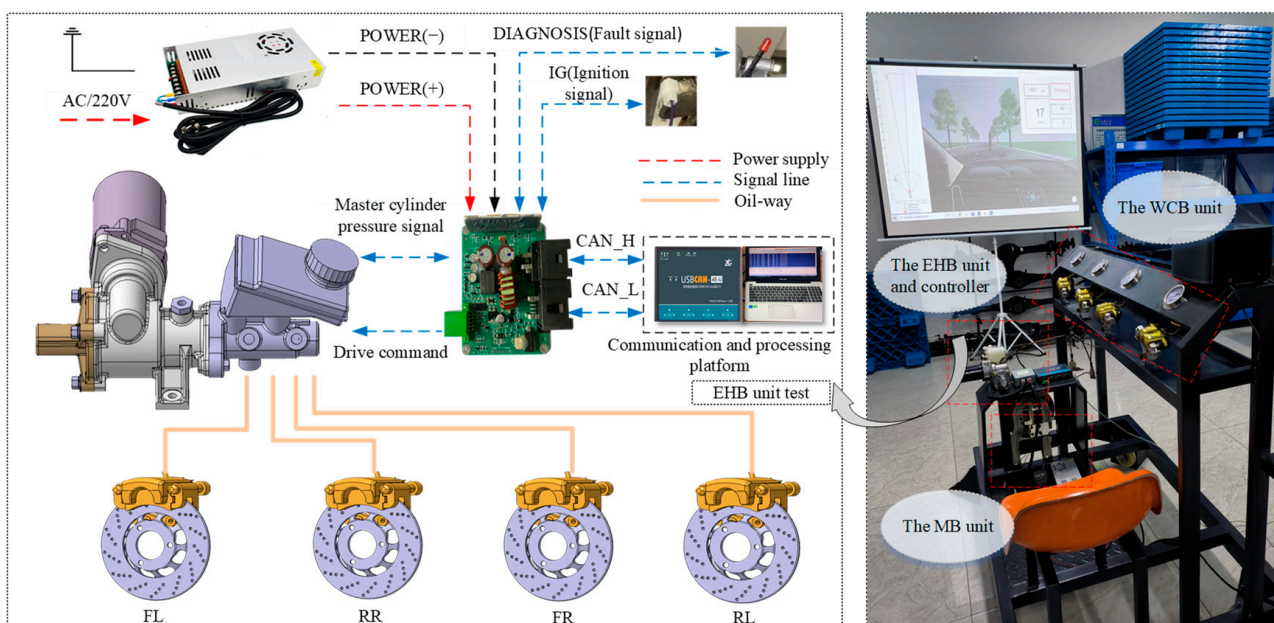

Figure 8. The HIL test rig.

Table 3. The specifications of the test rig.

Name	Specifications
Maximum pressure of the master cylinder	8 MPa
Rated voltage of the motor	12 V
Rated voltage of the oil pressure sensor	5 V
Rated voltage range of the controller	9–16 V
Baud rate of the CAN Bus analyser	500 kbs

Figure 9 shows the time–pressure history results of the step target pressure-tracking test. The pressure value of the master cylinder can coincide well with the target signal with 4 MPa and 6 MPa, respectively. The actual pressure overshoot of the test is kept within 0.6 MPa, and the steady-state error is kept within 0.3 MPa, which meets the basic requirements of the HMRSB for braking efficiency.
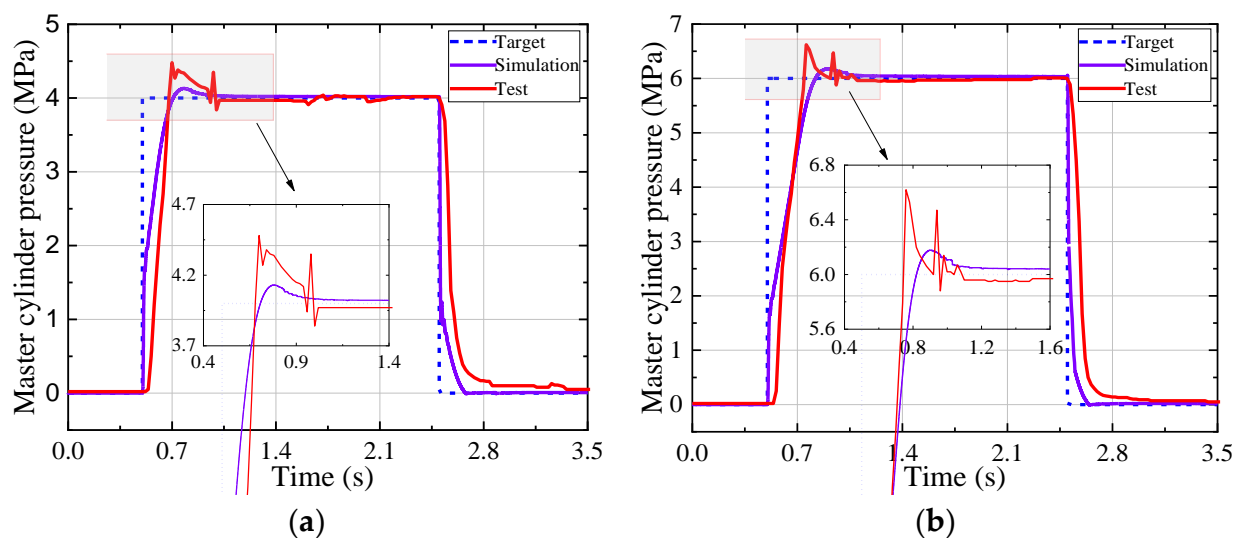
Figure 9. The test results of the step target pressure: (**a**) amplitude 4 MPa; and (**b**) amplitude 6 MPa.

The test results of the sine target pressure tracking are provided in Figure 10. Different signal offsets (2 MPa and 3 MPa), amplitude (2 MPa and 3 MPa), and frequency (0.5 Hz and 1 Hz) were set in the test. The results show that the pressure of the master cylinder has high accuracy in tracking the periodic dynamic target pressure. The maximum tracking error between the actual and target values is within 0.7 MPa, which appears in Figure 10d. However, there are also shortcomings, such as fluctuations of the pressure signal intermittently, which are proportional to the target pressure amplitude and frequency. The fluctuations in all the tests are mainly due to the uncertain frictional characteristics of the actual transmission components, which are not considered in the simulation model.

5.2. Test Vehicle Test Results

An LSEV (sightseeing vehicle) was retrofitted with the HMRBS proposed in this paper to verify its braking performance in the road test, shown in Figure 11. A high-precision GPS/IMU system was used to obtain the braking deceleration, vehicle speed, and braking distance. The relevant requirements for road tests mainly refer to GB/T 21268-2014 and GB/T 7258-2017 [27,28].
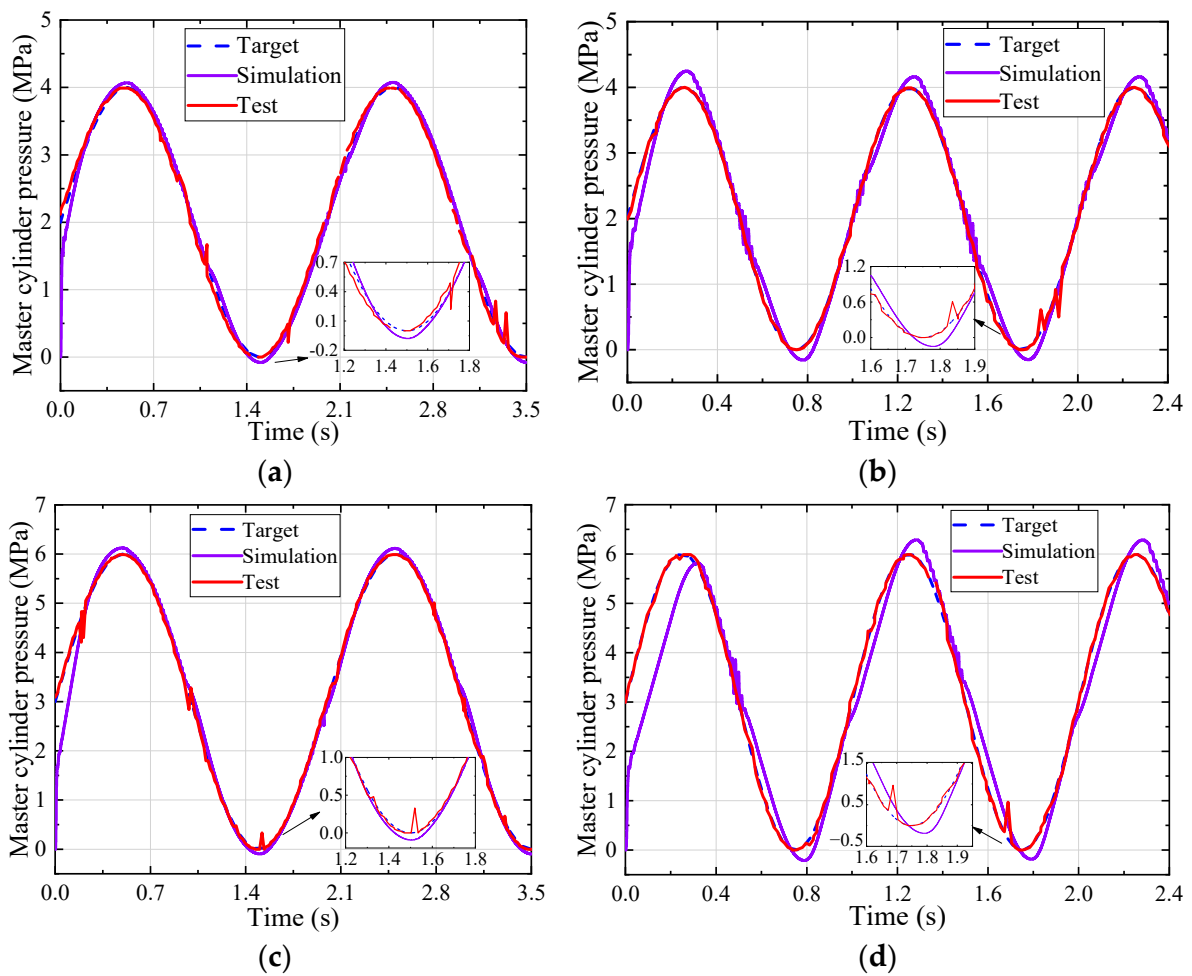
Figure 10. The sinusoidal target pressure test results: (**a**) amplitude 2 MPa, frequency 0.5 Hz; (**b**) amplitude 2 MPa, frequency 1 Hz; (**c**) amplitude 3 MPa, frequency 0.5 Hz; and (**d**) amplitude 3 MPa, frequency 1 Hz.

Figure 11. A test LSEV equipped with HMRBS. 1—Sightseeing vehicle; 2—HMRBS; 3—Test road; 4—High precision GPS/IMU system and CAN data analyser.

Considering that the test vehicle is used in a closed scenario, the maximum braking pressure of the master cylinder is limited to 4 MPa, and it can meet the vehicle braking demand. During the test, the vehicle was accelerated to 30 km/h and then held at a constant speed for a while before the brakes were applied. Emergency and mild brakes with active and manual braking modes were applied to evaluate the braking performance in different conditions.

The dynamic response of active and manual braking modes in the emergency braking condition is presented in Figure 12. The master cylinder pressure and deceleration generated by the EHB unit increased stably. The speed slowed down linearly, indicating that the EHB unit is reliable and effective in the active braking mode. The manual braking mode has the same deceleration trend as the active braking mode. It indicates that the modification does not affect the manual braking performance. Therefore, the MB unit can be used as a backup of the EHB unit, and the design enables dual braking and independent control.
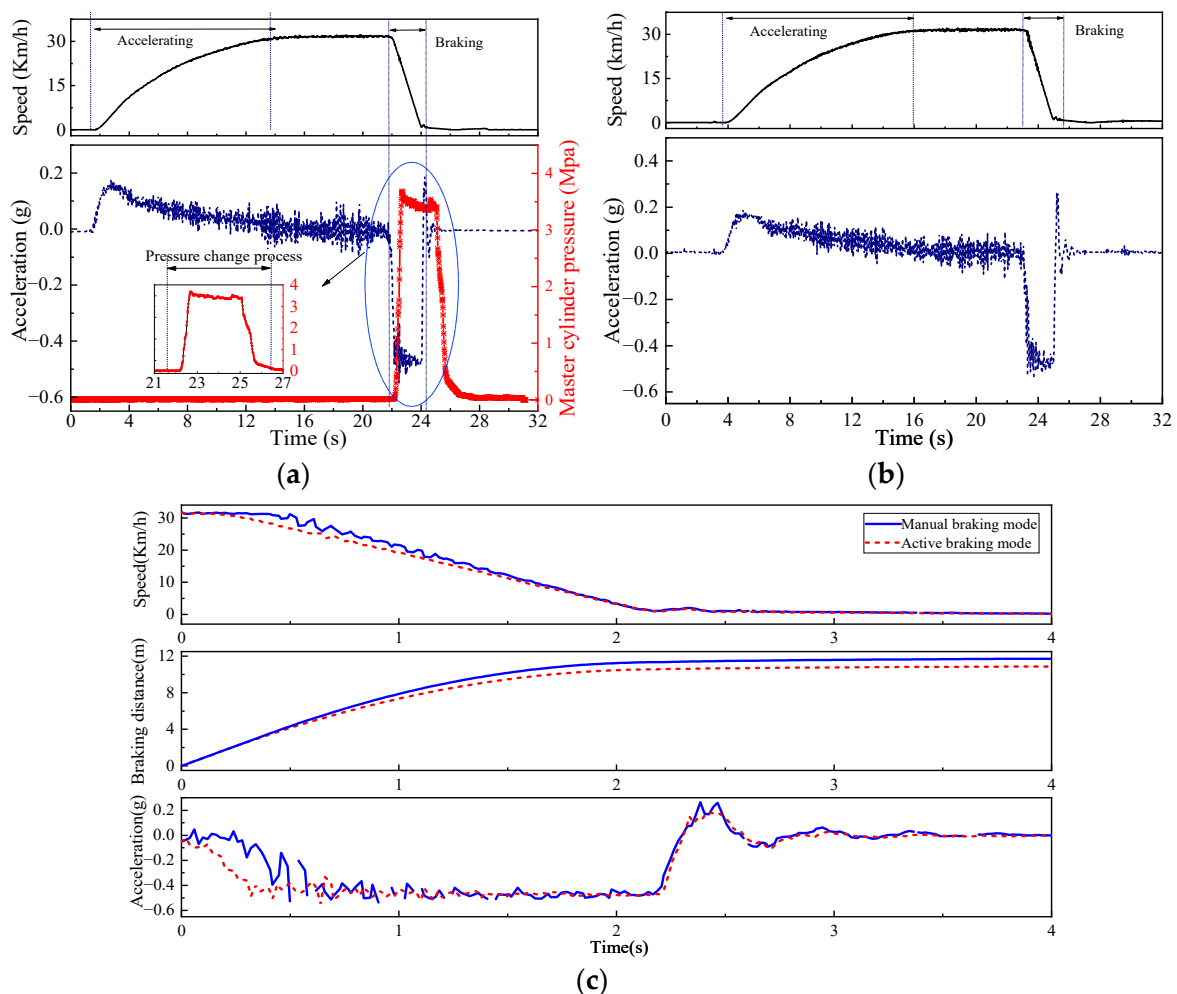

Figure 12. Emergency braking test: (**a**) active braking mode; (**b**) manual braking mode; and (**c**) comparison of vehicle dynamics characteristics.

Figure 12c illustrates the vehicle speed, acceleration, and braking distance after the HMRBS receives the brake signal. The braking deceleration fluctuates around −0.5 g, and the braking time is about 2.2 s in both braking modes. But the braking distance of the manual and active braking modes is 11.5 m and 10.8 m, respectively. Moreover, the deceleration fluctuation generated by the EHB unit is smaller than that of the MB unit. Therefore, the active braking mode is more stable and effective.

The dynamic response of active and manual braking modes in the mild braking condition is presented in Figure 13. The braking distance of the manual and active braking modes is about 20.4 m and 13.6 m, respectively. The braking deceleration fluctuates around −0.2 g and −0.35 g, and the braking time is 4.7 s and 2.9 s, respectively. The EHB unit produces fewer deceleration fluctuations than the MB unit, and the braking force is more stable.
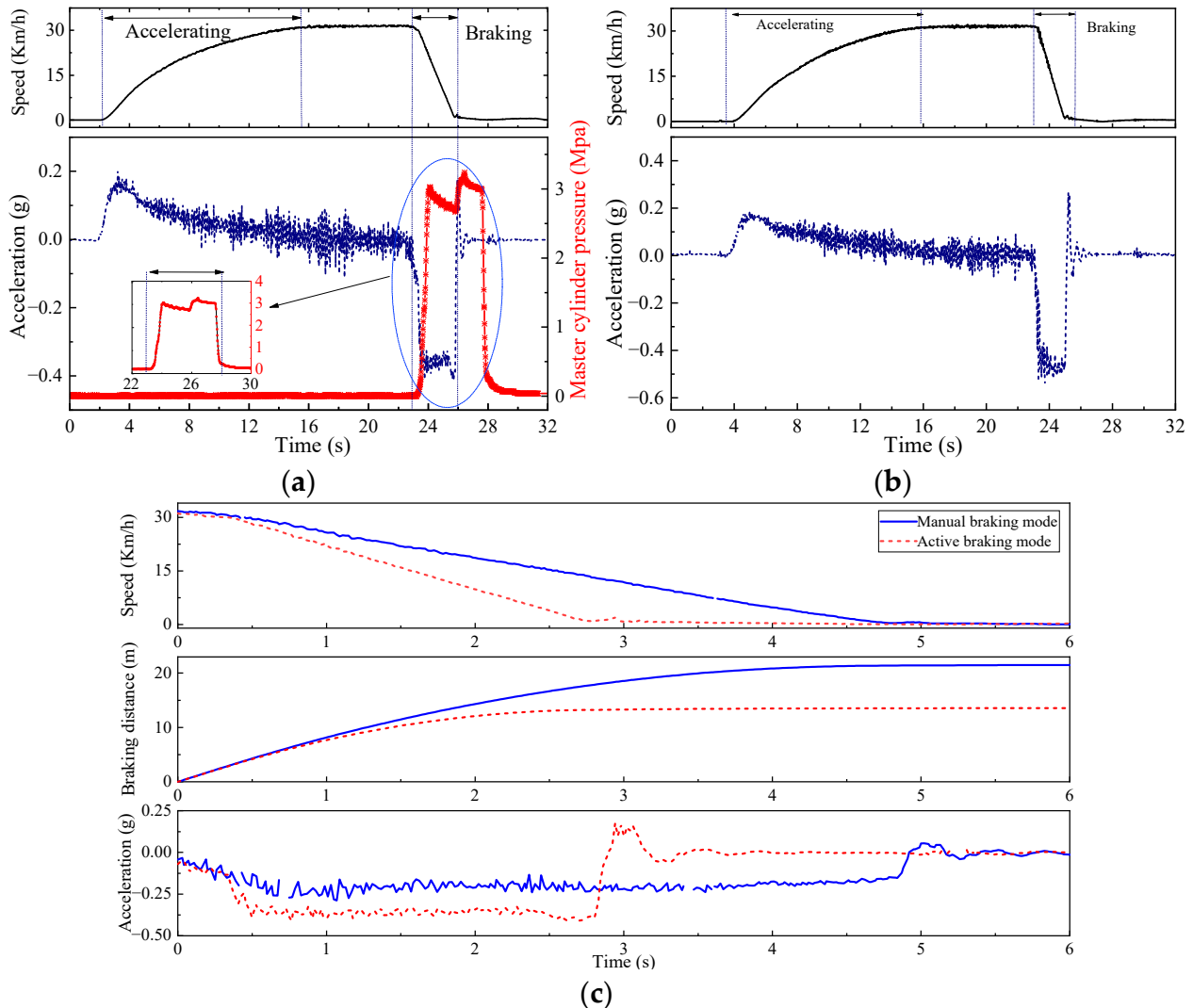

Figure 13. Mild braking test: (**a**) active braking mode; (**b**) manual braking mode; and (**c**) comparison of vehicle dynamics characteristics.

Therefore, the EHB unit is superior to the MB unit in response speed and braking efficiency in the HMRBS, and the braking effect is more stable. Furthermore, on the premise of retaining the original braking system, the low-cost HMRBS ensures the redundancy of braking backup in case of power failure of the EHB unit. It can meet the braking performance and safety requirements of the LSEV.

6. Conclusions

1. An HMRBS with a simple structure, high reliability, low cost, easy modification, and low debugging difficulty for aftermarket LSEVs has been proposed in this paper. The HMRBS retains the original braking system of the LSEV. It can realise the vehicle braking backup redundancy ability and improve active safety.

2. A master cylinder pressure controller with adaptive fuzzy PID and a servo motor speed controller with double-closed-loop PI have been designed to improve the system response performance. Simulation and test rig experiments have validated the feasibility and pressure-tracking performance. The dynamic pressure-tracking error is less than 0.6 MPa, and the steady-state error is within 0.3 MPa.

3. An LSEV has been retrofitted with an HMRBS to verify its braking performance in the road test. As a result, the maximum braking deceleration of both manual and active braking modes can reach −0.5 g. Significantly, the deceleration fluctuation and braking distance of the EHB unit are smaller than that of the MB unit, and its braking effect is more stable.

Author Contributions: Conceptualisation, C.W. and S.S.; experiment and data analysis, W.Q., L.C. and G.T.; writing, S.S., Y.T. and K.L.; resources, P.D.; revision, X.H. and C.W.; funding acquisition, S.S. All authors have read and agreed to the published version of the manuscript.

Data Availability Statement: The datasets used and analysed during the current study are available from the corresponding author upon reasonable request.

Conflicts of Interest: The authors declare no conflict of interest.

Abbreviation

HMRBS	Human–machine redundant braking system
LSEVs	Low-speed electric vehicles
EHB	Electro-hydraulic braking
MB	Manual braking
PID	Proportion integration differentiation
PI	Proportion integration
ADAS	Advanced driver assistance systems
ACC	Adaptive cruise control
AEB	Autonomous emergency braking
WCB	Wheel cylinder braking
CAN	Controller area network
BLDCM	Brushless DC motor
WGR	Worm gear reducer
BSM	Ball screw mechanism
MC	Master cylinder
SV	Shuttle valves
PS	Pressure sensor
BP	Brake pedal
PDS	Pedal displacement sensor
FL	Caliper assembly—front left
FR	Caliper assembly—front right
RR	Caliper assembly—rear left
RL	Caliper assembly—rear left

References

1. Chiara, F.; Canova, M. A review of energy consumption, management, and recovery in automotive systems, with considerations of future trends. *Proc. Inst. Mech. Eng. Part D J. Automob. Eng.* **2013**, *227*, 914–936. [CrossRef]
2. Giuseppe, A.P.; Giovanni, B. Multi-objective optimal computer-aided engineering of hydraulic brake systems for electrified road vehicles. *Veh. Syst. Dyn.* **2020**, *60*, 391–412.
3. Meng, B.; Yang, F.; Liu, J.; Wang, Y. A survey of brake-by-wire system for intelligent connected electric vehicles. *IEEE Access* **2020**, *8*, 225424–225436. [CrossRef]
4. Li, X.; Lin, K.-Y.; Meng, M.; Li, X.; Li, L.; Hong, Y.; Chen, J. A survey of adas perceptions with development in China. *IEEE Trans. Intell. Transp. Syst.* **2022**, *23*, 14188–14203. [CrossRef]

5. Yu, Z.; Xu, S.; Lu, X.; Wei, H. An integrated-electro-hydraulic brake system for active safety. In Proceedings of the SAE 2016 World Congress and Exhibition, Detroit, MI, USA, 12–14 April 2016.

6. Kin, K.; Yano, O.; Urabe, H. Enhancements in vehicle stability and steerability with VSA. In Proceedings of the Transportation and Logistics Conference, Tokyo, Japan, 4 December 2001.

7. Wu, Z.; Ma, Q.; Li, C. Performance investigation and analysis of market-oriented low-speed electric vehicles in China. *J. Clean. Prod.* **2015**, *91*, 305–312. [CrossRef]

8. Gong, X.; Ge, W.; Yan, J.; Zhang, Y.; Gongye, X. Review on the development, control method and application prospect of brake-by-wire actuator. *Actuators* **2020**, *9*, 15. [CrossRef]

9. Shi, B.; Xiong, L.; Yu, Z. Pressure estimation of the electro-hydraulic brake system based on signal fusion. *Actuators* **2021**, *10*, 240. [CrossRef]

10. Feigel, H. Integrated brake system without compromises in functionality. *ATZ Worldwide* **2012**, *114*, 46–50. [CrossRef]

11. Riese, C.; Gauterin, F. Analysis of hydraulic brake systems with regard to the requirements for future vehicle concept. In Proceedings of the Internationales Stuttgarter Symposium: Automobil-und Motorentechnik, Stuttgart, Germany, 15–16 March 2016.

12. Xiong, L.; Han, W.; Yu, Z.; Lin, J.; Xu, S. Master cylinder pressure reduction logic for cooperative work between electro-hydraulic brake system and anti-lock braking system based on speed servo system. *Proc. Inst. Mech. Eng. Part D J. Automob. Eng.* **2020**, *234*, 3042–3055. [CrossRef]

13. Li, C.; Zhang, J.; Hou, X.; Ji, Y.; Han, J.; He, C.; Hao, J. A novel double redundant brake-by-wire system for high automation driving safety: Design, optimisation and experimental validation. *Actuators* **2021**, *10*, 287. [CrossRef]

14. Yuan, C.; He, Z.; Shen, J.; Chen, L.; Cai, Y.; He, Y.; Weng, S.; Yuan, Y.; Gong, Y. Design, modeling, and simulation of dual-source redundant braking system. *Proc. Inst. Mech. Eng. Part D J. Automob. Eng.* **2022**. [CrossRef]

15. Todeschini, F.; Corno, M.; Panzani, G.; Fiorenti, S.; Savaresi, S.M. Adaptive cascade control of a brake-by-wire actuator for sport motorcycles. *IEEE-ASME Trans. Mechatron.* **2015**, *20*, 1310–1319. [CrossRef]

16. Zhao, J.; Chen, Z.; Zhu, B.; Wu, J. Precise active brake-pressure control for a novel electro-booster brake system. *IEEE Trans. Ind. Electron.* **2020**, *67*, 4774–4784. [CrossRef]

17. Chen, Q.; Shao, H.; Liu, Y.; Xiao, Y.; Wang, N.; Shu, Q. Hydraulic-pressure-following control of an electronic hydraulic brake system based on a fuzzy proportional and integral controller. *Eng. Appl. Comp. Fluid Mech.* **2020**, *14*, 1228–1236. [CrossRef]

18. Sain, C.; Banerjee, A.; Biswas, P.K.; Azar, A.T.; Babu, T.S. Design and optimisation of a fuzzy-PI controlled modified inverter-based PMSM drive employed in a light weight electric vehicle. *Int. J. Autom. Control* **2022**, *16*, 459–488. [CrossRef]

19. Sain, C.; Banerjee, A.; Kumar Biswas, P.; Sudhakar Babu, T.; Dragicevic, T. Updated PSO optimised fuzzy-PI controlled buck type multi-phase inverter-based PMSM drive with an over-current protection scheme. *IET Electr. Power Appl.* **2020**, *14*, 2331–2339. [CrossRef]

20. Chen, Q.; Liu, Y.; Zeng, L.; Xiao, Q.; Zhou, C.; Kang, S. On the control of the master cylinder hydraulic pressure for electro-hydraulic brake (EHB) systems with the sliding mode design methodology. *Fluid Dyn. Mater. Process.* **2018**, *14*, 281–291. [CrossRef]

21. Shi, T.; Niu, X.; Chen, W.; Xia, C. Commutation torque ripple reduction of brushless dc motor in braking operation. *IEEE Trans. Power Electron.* **2018**, *33*, 1463–1475. [CrossRef]

22. Merritt, H.E. *Hydraulic Control Systems*; Wiley: New York, NY, USA, 1967; p. 35.

23. Wang, C.; Zhao, W.; Li, W.; Yu, L. Multi-objective optimisation of electro-hydraulic braking system based on moea/d algorithm. *IET Intell. Transp. Syst.* **2019**, *13*, 183–193. [CrossRef]

24. Liu, J. *Intelligent Control*, 4th ed.; Publishing House of Electronics Industry: Beijing, China, 2017.

25. Liu, Y.; Lei, Y.; Fan, J.; Wang, F. Survey on image classification technology based on small sample learning. *Acta Autom. Sin.* **2021**, *47*, 297–315.

26. Jiang, H.; Jie, W.; Hui, F. An anti-windup self-tuning fuzzy pid controller for speed control of brushless dc motor. *Automatika* **2017**, *58*, 321–335. [CrossRef]

27. *GB/T 21268-2014*; General Technical Conditions for Garden Patrol Minibus. China National Standardization Administration: Beijing, China, 2014.

28. *GB 7258-2017/XG2-2021*; Technical Specifications for Safety of Power-Driven Vehicles Operating on Roads. China National Standardization Administration: Beijing, China, 2017.